One-pot synthesis of azabora[6]helicene by a Schiff base forming reaction

Kage, Yuto
Department of Applied Chemistry, Graduate School of Engineering and Centre for Molecular Systems, Kyushu University

Jiang, Yuchuan
Department of Applied Chemistry, Graduate School of Engineering and Centre for Molecular Systems, Kyushu University

Minakuchi, Namiki
Department of Applied Chemistry, Graduate School of Engineering and Centre for Molecular Systems, Kyushu University

Mori, Shigeki
Advanced Research Support Centre (ADRES), Ehime University

他

出版情報：Chemical Communications. 60 (26), pp.3543-3546, 2024-03-02. Royal Society of Chemistry (RSC)
バージョン：
権利関係：

COMMUNICATION

One-pot synthesis of azabora[6]helicence by a Schiff base forming reaction

Received 00th January 20xx,
Accepted 00th January 20xx

DOI: 10.1039/x0xx00000x

Yuto Kage,[a] Yuchuan Jiang,[a] Namiki Minakuchi,[a] Shigeki Mori[b] and Soji Shimizu*[a]

Azabora[6]helicene as a new heterohelicene analogue was synthesized by a one-pot reaction of commercially available 2,6-diaminopyridine and benzo[*c*,*d*]indole-2(1H)-one and subsequent boron coordination. While the single crystal X-ray diffraction analysis elucidated a helical structure in the solid state, a dynamic helicity inversion was observed in a solution.

[*n*]Helicenes, polyaromatic hydrocarbons comprising the number "*n*" of *ortho*-fused aromatic rings,[1,2] have been attracting attention because of their inherent helical chirality for applications as chiral ligands in asymmetric syntheses[3,4] and chiroptical properties such as circular dichroism (CD) and circularly polarized luminescence (CPL) for optoelectronics applications.[5–7] To modulate and enhance the chiroptical properties, the introduction of heteroatoms into the helicene structures has been attempted.[8] Among so-called heterohelicenes, boron-containing helicenes (borahelicenes), in which nitrogen or oxygen atoms are also doped in the structures to coordinate and stabilize the boron atoms, have recently been recognized as a unique class of heterohelicenes because of their improved fluorescence efficiency and the Lewis acidity of the boron atoms.[9–12] Borahelicenes were conventionally synthesized by C–H borylation using other heteroatoms such as nitrogen and oxygen atoms as directing groups. As a novel synthetic methodology of borahelicenes, herein, we report a one-pot synthesis based on a Schiff base forming reaction using commercially available 2,6-diaminopyridine and benzo[*c*,*d*]indole-2(1H)-one.

Recently, we have developed the Schiff base forming reaction of azaarylamines and lactams to synthesize azaborondipyrromethenes (aza-BODIPYs).[13] In this reaction, using lactam compounds bearing two lactam moieties, such as diketopyrrolopyrrole,[14] benzodipyrrolidone,[15,16] and isoindigo,[15] π-extended dimeric aza-BODIPYs can be synthesized. Owing to their prominent optical properties in the far-red and near-infrared (NIR) regions, the applications in various fields such as bioimaging,[17] molecular recognition,[18] organic photovoltaics,[19] organic light emitting diodes,[20] electrochemiluminescence[21] and nonlinear optics[22] have been extensively investigated. During the synthetic studies on these aza-BODIPYs, we noticed that our synthetic strategy could also be applied to construct a structure of azabora[6]helicene as a novel heterohelicene when 2,6-diaminopyridine is used instead of azaarylmonoamines.

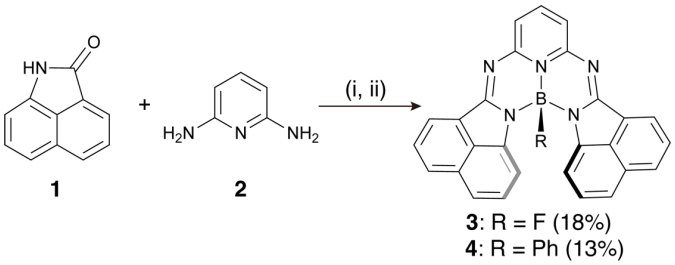

Scheme 1 Synthesis of azabora[6]helicenes, **3** and **4**. Reaction conditions (i): $TiCl_4$, NEt_3, toluene, reflux; (ii) $BF_3{\cdot}OEt_2$ for **3** and (i) $TiCl_4$, NEt_3, *o*-DCB, reflux; (ii) $BPh_3{\cdot}PPh_3$, NEt_3 for **4**.

Azabora[6]helicene **3** was synthesized from a Schiff base forming reaction of benzo[*c*,*d*]indole-2(1H)-one **1** and 2,6-diaminopyridine **2** in the presence of titanium tetrachloride and triethylamine in toluene under refluxing conditions and subsequent boron coordination using $BF_3{\cdot}OEt_2$. Purification by silica gel column chromatography provided **3** with a fluorine axial ligand on the central boron atom in 18% yield (Scheme 1). An axially phenyl-substituted derivative (**4**) was also similarly synthesized in 13% yield using *o*-dichlorobenzene (*o*-DCB) as a

[a] *Department of Applied Chemistry, Graduate School of Engineering and Centre for Molecular Systems, Kyushu University, Fukuoka 819-0395, Japan. E-mail: ssoji@cstf.kyushu-u.ac.jp*
[b] *Advanced Research Support Centre (ADRES), Ehime University, Matsuyama 790-8577, Japan.*

† Footnotes relating to the title and/or authors should appear here.
Electronic Supplementary Information (ESI) available: [details of any supplementary information available should be included here]. See DOI: 10.1039/x0xx00000x

solvent and triphenylborane-triphenylphosphine complex (BPh_3·PPh_3) as a boron reagent. The structures of **3** and **4** were characterized by high-resolution mass spectrometry, ^1H and ^{19}F NMR spectroscopy

and single-crystal X-ray diffraction analysis (Figs. 1 and S1–S8). Both compounds were crystallized in a $\overline{P}1$ space group as a racemic mixture of enantiomers with *P*- and *M*-helicities (Table S1). The biting angles of **3** and **4** between benzo[*c*,*d*]indole moieties are 46° and 38°, respectively. In the crystal packing diagram of **3**, the benzoindole moieties of *P*- and *M*-enantiomers form π-π stacking, resulting in a one-dimensional columnar arrangement of **3** along the *a*-axis.

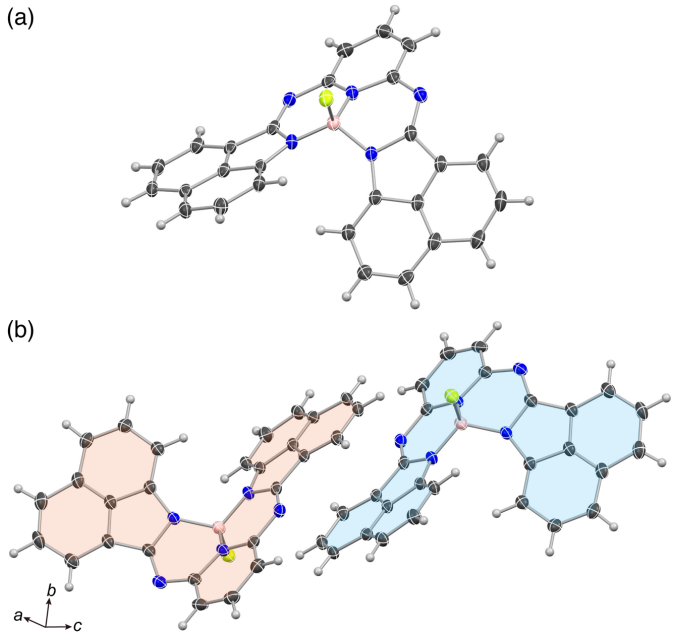

Fig. 1 X-ray single crystal structures of **3**: (a) *P*-enantiomer and (b) packing diagram in which the *P*- and *M*-enantiomers are highlighted in blue and orange, respectively. The thermal ellipsoids are scaled to the 50% probability level.

The variable-temperature (VT) ^1H NMR studies in 1,1,2,2-tetrachloroethane-d_2 revealed the dynamic helicity inversion of **3** for racemization: at room temperature, **3** exhibited signals for the fifteen protons in the aromatic regions (8.71 (1H), 8.52 (1H), 8.26 (2H), 8.12 (1H), 7.93 (2H), 7.83 (1H), 7.75 (2H), 7.68 (1H), 7.52 (1H), 7.47 (1H), 6.97 (1H) and 6.56 (1H) ppm), whereas upon elevating temperature, pairs of signals due to the benzo[*c*,*d*]indole and pyridine moieties coalesced to merge into single signals (Figs. 2 and S9). The line-shape analyses of the VT ^1H NMR spectra using three pairs of the benzo[*c*,*d*]indole proton signals as designated in Fig. S10 determined the inversion rate (*k*) at each temperature and activation parameters: E_a = 13.30 kcal mol^{-1}, $\Delta H^{\ddagger}$ = 12.66 kcal mol^{-1}, $\Delta S^{\ddagger}$ = –9.98 cal mol^{-1} K^{-1} and $\Delta G^{\ddagger}_{298}$= 15.70 kcal mol^{-1} for **3** (Figs. S11–S15 and Tables S2 and S3). DFT calculations were performed at the B3LYP/6-311G(2d,p) level to estimate the thermodynamic parameters for the helicity inversion. The calculated activation barrier at 298 K is $\Delta G^{\ddagger}$ = 14.8 kcal mol^{-1}, and the corresponding thermodynamic parameters are $\Delta H^{\ddagger}$ = 13.8 kcal mol^{-1} and $\Delta S^{\ddagger}$ = –3.5 cal mol^{-1} K^{-1} (Fig. 3). From these parameters, the half-life of the helicity inversion process of **3** is calculated to be 16 msec at 298 K. These calculated values for the helicity inversion processes agree well with those based on the ^1H NMR simulation. The estimated activation energies are small enough for racemization at room temperature, which prevents us from isolation of enantiomers by chiral HPLC.

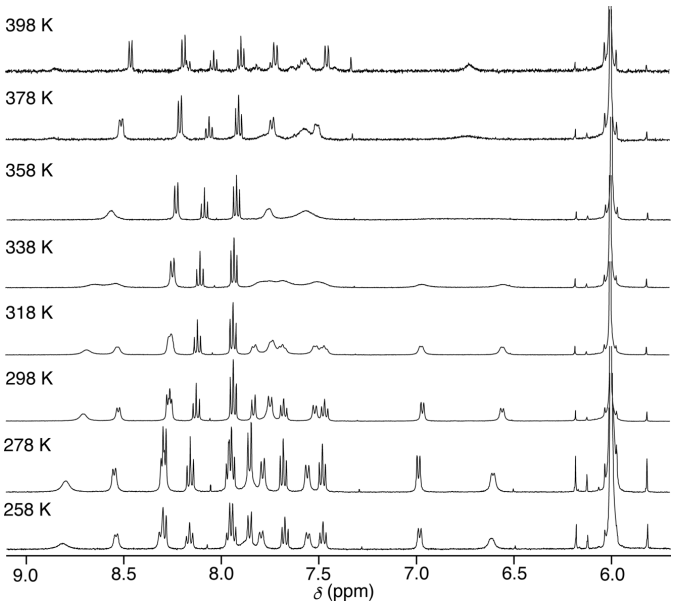

Fig. 2 VT ^1H NMR spectra of **3** in 1,1,2,2-tetrachloroethane-d_2.

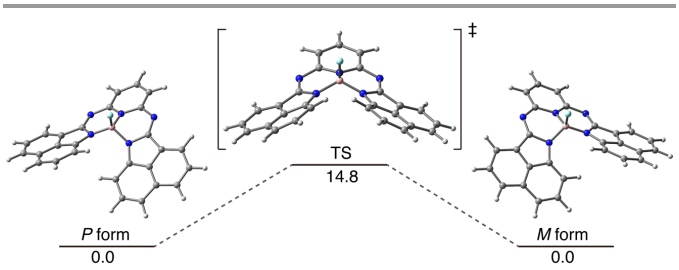

Fig. 3 Relative Gibbs free energy diagram for the racemization process of **3** (kcal mol^{-1}) calculated at the B3LYP/6-311G(2d,p) level of theory.

In chloroform, **3** shows intense absorption with several bands at 548, 513, 437 and 415 nm in the visible region (Fig. 4 and Table 1). **4** also exhibits similar absorption spectrum, indicating the minor effect of the axial ligand on the electronic structure of azabora[6]helicene (Fig. S16). Compared with the absorption spectrum of aza-BODIPY analogue (**5**) comprising benzo[*c*,*d*]indole and pyridine units as a half structure of **3**,[23,24] the lowest energy bands show redshifts due to the extension of the π-conjugation. The fluorescence spectrum of **3** is a mirror image to the absorption spectrum, exhibiting well-structured spectral profile with the fluorescence maximum at 568 nm and a vibronic band at 610 nm. The fluorescence quantum yields of **3** and **4** are 0.26 and 0.18, respectively, which are moderately high as a borahelicene compound, but smaller than that of **5** (0.83). The deterioration of the fluorescence quantum yields from **5** can be ascribed to the molecular vibration arising from the helical structure, which enhances the nonradiative decay processes. The solid-state emission property of **5** due to

Table 1 Optical and electrochemical properties of **3** and **4**.

Compd	λ [nm] (10^{-4} ε [M^{-1} cm^{-1}])	$\lambda_{Fl/CHCl_3}$ [nm]	$\phi_{Fl/CHCl_3}$	$\lambda_{Fl/film}$[a] [nm]	$\phi_{Fl/film}$[a]	E_{ox}[b] [V]	E_{red}[c] [V]
3	548 (1.90), 513 (1.82), 437 (2.03), 415 (2.78)	568	0.26	667	0.02	0.64	–1.94, –2.20
4	554 (1.60), 518 (1.48), 442 (2.80), 417 (2.20)	574	0.18	632	0.04	0.63	–1.82, –2.18

[a]Fluorescence maximum and quantum yields measured in an amorphous drop-cast film. [b]Peak potentials (V vs. Fc^+/Fc) measured by DPV in *o*-DCB with TBAP. [c]Half-wave potentials (V vs. Fc^+/Fc) measured by CV in *o*-DCB with TBAP.

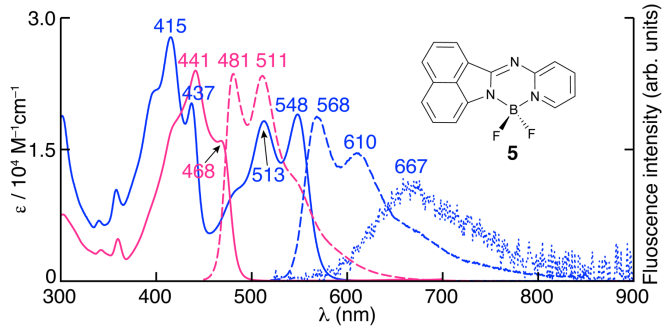

Fig. 4 UV/vis absorption (solid line) and fluorescence (dashed line) spectra of **3** (blue line) and **5** (pink line) as a reference compound in chloroform and fluorescence spectrum of **3** in a drop-cast film (blue dotted line). The structure of **5** is shown in the inset.

the large apparent Stokes shift was reported.[23,24] Despite the similar component units, the fluorescence emission of **3** and **4** is virtually quenched in a film state with fluorescence quantum yields of 0.02 and 0.04, respectively (Figs. 4 and S16). This is explained in terms of the small Stokes shift, which enhances self-absorption quenching in a film state.

To give detailed insight into the electronic structures of azabora[6]helicene, theoretical calculations based on the DFT method at the B3LYP/6-311G(2d,p) level of theory were performed (Fig. 5 and Tables S4 and S5). In the frontier molecular orbitals (MOs) of **3**, the HOMO and HOMO–1, and the LUMO and LUMO+1 can be recognized as a linear combination of the HOMO and LUMO of **5**, respectively, resulting in the significant destabilization of the HOMO and slight destabilization of the LUMO from those of **5**. The TDDFT calculation reveals two main excited states (S1 and S3) with large oscillator strengths of 0.254 and 0.287, respectively. The HOMO-to-LUMO transition exclusively contributes to the S1 state, whereas the S3 state comprises a transition from HOMO–1 to LUMO and one from HOMO to LUMO+1. Based on this theoretical absorption, the absorption bands of **3** at 548 and 437 nm can be assigned to the S0-S1 and S0-S3 transitions, respectively, and the other bands at 513 and 415 nm are their vibronic bands.

Cyclic and differential pulse voltammograms (CV and DPV) of **3** and **4** were measured using a 0.5 mM sample solution in *o*-dichlorobenzene (*o*-DCB) containing 0.1 M tetra-*n*-butylammonium perchlorate (TBAP) as a supporting electrolyte (Figs. 6 and S17). **3** exhibits a pseudo-reversible oxidation wave at 0.64 V vs. Fc^+/Fc and two reversible reduction waves at –1.94 and –2.20 V. **4** also has similar redox potentials. The HOMO-LUMO energy gap of **3** estimated from the oxidation and first reduction potentials is 2.58 eV, which is slightly larger than that of the optical band gap (2.15 eV).

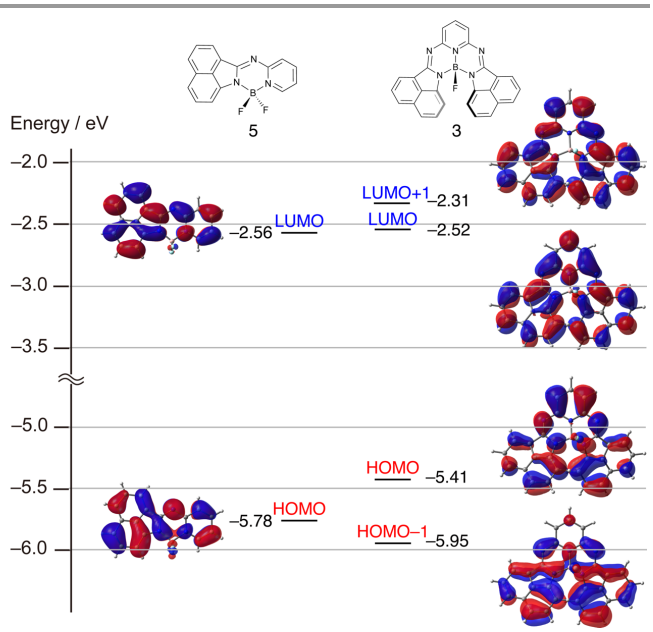

Fig. 5 Partial frontier molecular orbital diagrams of **3** (right) and **5** (left) at the B3LYP/6-311G(2d,p) level of theory.

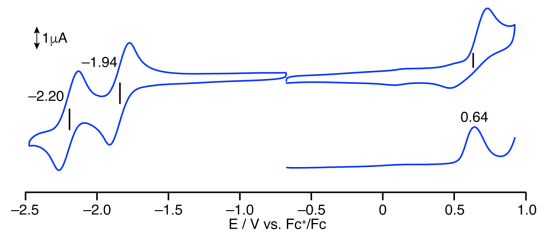

Fig. 6 CV and DPV of **3** (0.5 mM) in *o*-DCB containing 0.1 M TBAP (scan rare: 100 mV s^{-1} for CV; pulse amplitude: 0.05 V, pulse width: 0.2 s for DPV).

In summary, we have reported the synthesis of azabora[6]helicene as a novel heterohelicene analogue. The helical structure of azabora[6]helicene is induced by the coordination geometry of the central boron atom and the steric hindrance of the terminal benzo[*c*,*d*]indole moieties. Although the helical structure was confirmed by single crystal X-ray diffraction analysis, the dynamic helicity inversion in solution due to the small activation energy for racemization has hampered the isolation of the enantiomers. The introduction of bulky substituents to the peripheral positions may fix the helical structure, enabling optical resolution by chiral HPLC. In addition,

azabora[6]helicene can be a precursor of a triphyrin analogue,[25,26] which is a macrocyclic compound comprising three heteroaromatic ring units such as pyrrole and pyridine. Further studies on the peripheral functionalization of azabora[6]helicene to those ends are being intensively investigated in our lab and will be reported in due course.

This work was financially supported by a Grant-in-Aid from JSPS (No. JP 22H020640) and the Asahi Glass Foundation. The authors thank Prof. Hiroyuki Furuta at Ritsumeikan University for his insightful suggestions.

Conflicts of interest

There are no conflicts to declare.

Notes and references

1 Y. Shen and C.-F. Chen, *Chem. Rev.*, 2012, **112**, 1463–1535.
2 M. Gingras, *Chem. Soc. Rev.*, 2013, **42**, 1051–1095.
3 K. Yavari, P. Aillard, Y. Zhang, F. Nuter, P. Retailleau, A. Voituriez and A. Marinetti, *Angew. Chem. Int. Ed.*, 2014, **53**, 861–865.
4 M. J. Narcis and N. Takenaka, *Eur. J. Org. Chem.*, 2014, 21–34.
5 W.-L. Zhao, M. Li, H.-Y. Lu and C.-F. Chen, *Chem. Commun.* 2019, **55**, 13793–13803.
6 F. Furche, R. Ahlrichs, C. Wachsmann, E. Weber, A. Sobanski, F. Vögtle and S. Grimme, *J. Am. Chem. Soc.*, 2000, **122**, 1717–1724.
7 (a) Y. Nakakuki, T. Hirose, H. Sotome, M. Gao, D. Shimizu, R. Li, J. Hasegawa, H. Miyasaka and K. Matsuda, *Nat. Commun.,* 2022, **13**, 1475; (b) H. Kubo, T. Hirose, T. Nakashima, T. Kawai, J. Hasegawa and K. Matsuda, *J. Phys. Chem. Lett*., 2021, **12**, 686–695; (c) Y. Nakakuki, T. Hirose, H. Sotome, H. Miyasaka and K. Matsuda, *J. Am. Chem. Soc.*, 2018, **140**, 4317–4326.
8 K. Dhbaibi, L. Favereau and J. Crassous, *Chem. Rev.*, 2019, **119**, 8846–8953.
9 (a) S. Oda, B. Kawakami, Y. Yamasaki, R. Matsumoto, M. Yoshioka, D. Fukushima, S. Nakatsuka and T. Hatakeyama, *J. Am. Chem. Soc.*, 2022, **144**, 106–112; (b) T. Katayama, S. Nakatsuka, H. Hirai, N. Yasuda, J. Kumar, T. Kawai and T. Hatakeyama, *J. Am. Chem. Soc.*, 2016, **138**, 5210–5213; (c) T. Hatakeyama, S. Hashimoto, T. Oba and M. Nakamura, *J. Am. Chem. Soc.*, 2012, **134**, 19600–19603.
10 C. Shen, M. Srebro-Hooper, M. Jean, N. Vanthuyne, L. Toupet, J. A. G. Williams, A. R. Torres, A. J. Riives, G. Muller, J. Autschbach and J. Crassous, *Chem. –Eur. J.*, 2017, **23**, 407–418.
11 (a) X.-Y. Wang, X. Yao, A. Narita and K. Müllen, *Acc. Chem. Res.* 2019, **52**, 2491–2505; (b) X.-Y. Wang, X.-C. Wang, A. Narita, M. Wagner, X.-Y. Cao, X. Feng and K. Müllen, *J. Am. Chem. Soc.*, 2016, **138**, 12783–12786.
12 K. Yuan, D. Volland, S. Kirschner, M. Uzelac, G. S. Nichol, A. Nowak-Król and M. J. Ingleson, *Chem. Sci.*, 2022, **13**, 1136–1145.
13 S. Shimizu, *Chem. Commun.*, 2019, **55**, 8722–8743.
14 (a) S. Shimizu, T. Iino, A. Saeki, S. Seki and N. Kobayashi, *Chem. –Eur. J.*, 2015, **21**, 2893–2904; (b) S. Shimizu, T. Iino, Y. Araki and N. Kobayashi, *Chem. Commun.*, 2013, **49**, 1621–1623.
15 M. Tamada, T. Iino, Y. Wang, M. Ide, A. Saeki, H. Furuta, N. Kobayashi and S. Shimizu, *Tetrahedron Lett.*, 2017, **58**, 3151–3154.
16 Y. Wang, L. Chen, R. M. El-Shishtawy, S. G. Aziz and K. Müllen, *Chem. Commun.* 2014*,* **50**, 11540–11542.
17 (a) W. Li, L. Wang, C. Zhang, X. Ran, H. Tang and D. Cao, *J. Mater. Chem. C*, 2022, **10**, 5672–5683; (b) L. Li, L. Wang, H. Tang and D. Cao, *Chem. Commun.*, 2017, **53**, 8352–8355.
18 (a) L. Wang, S. Xin, C. Zhang, X. Ran, H. Tang and D. Cao, *J. Mater. Chem. B*, 2021, **9**, 9383–9394; (b) W. Li, H. Zhao, R. Zhuang, Y. Wang, W. Cao, Y. He, Y. Jiang, R. Rui and S. Ju, *Theriogenology*, 2021, **164**, 1–11; (c) L. Wang, X. Ran, H. Tang and D. Cao, *Dyes Pigments*, 2021, **194**, 109634; (d) L. Li, W. Li, L. Wang, H. Tang, D. Cao and X. Ran, *Sens. Actuators B Chem.*, 2020, **312**, 127953; (e) L. Wang, H. Ding, H. Tang, D. Cao and X. Ran, *Anal. Chim. Acta*, 2020, **1135**, 38–46; (f) L. Li, W. Li, X. Ran, L. Wang, H. Tang and D. Cao, *Chem. Commun.*, 2019, **55**, 9789–9792.
19 (a) R. Feng, N. Sato, T. Yasuda, H. Furuta and S. Shimizu, *Chem. Commun.*, 2020, **56**, 2975–2978; (b) R. Feng, N. Sato, M. Nomura, A. Saeki, H. Nakanotani, C. Adachi, T. Yasuda, H. Furuta and S. Shimizu, *J. Mater. Chem. C*, 2020, **8**, 8770–8776.
20 Y. Kage, S. Kang, S. Mori, M. Mamada, C. Adachi, D. Kim, H. Furuta and S. Shimizu, *Chem. –Eur. J.*, 2021, **27**, 5259–5267.
21 R. Ishimatsu, H. Shintaku, Y. Kage, M. Kamioka, S. Shimizu, K. Nakano, H. Furuta and T. Imato, *J. Am. Chem. Soc.*, 2019, **141**, 11791–11795.
22 Y. Zhou, C. Ma, N. Gao, Q. Wang, P.-C. Lo, K. S. Wong, Q.-H. Xu, T. Kinoshita and D. K. P. Ng, *J. Mater. Chem. B*, 2018, **6**, 5570–5581.
23 S. Shimizu , A. Murayama, T. Haruyama, T. Iino, S. Mori, H. Furuta and N. Kobayashi, *Chem. –Eur. J.*, 2015, **21**, 12996–13003.
24 C. Cheng, N. Gao, C. Yu, Z. Wang, J. Wang, E. Hao, Y. Wei, X. Mu, Y. Tian, C. Ran and L. Jiao, *Org. Lett.* 2015, **17**, 278–281.
25 S. Shimizu, *Chem. Rev.*, 2017, **117**, 2730–2784.
26 G. Lavarda, J. Labella, M. V. Martínez-Díaz, M. S. Rodríguez-Morgade, A. Osuka and T. Torres, *Chem. Soc. Rev.*, 2022, **51**, 9482–9619.

